J Mater Sci: Mater Electron (2012) 23:1402–1408
DOI 10.1007/s10854-011-0605-5

Hydrothermal synthesis and mechanism and property study of La-doped $BiFeO_3$ crystallites

Zhiwu Chen · Yunfeng Li · Yongpeng Wu · Jianqiang Hu

Received: 15 September 2011 / Accepted: 13 December 2011 / Published online: 21 December 2011

Abstract Lanthanum-doped bismuth ferrite ($Bi_{1-x}La_xFeO_3$, wherein x is equal to 0, 0.15, 0.3, and 0.4) crystallites were synthesized by hydrothermal method. In the synthesis, precursor composition, potassium hydroxide concentration, and hydrothermal temperature and time played important roles in the crystallinity and morphology of $Bi_{1-x}La_xFeO_3$ crystallites. Pure $Bi_{1-x}La_xFeO_3$ crystallites could be obtained when $x < 0.3$, and ferroelectric transition temperature decreased from 834.2 to 828.7 °C with increasing La doping. The growth mechanism of the $Bi_{1-x}La_xFeO_3$ crystallines was also discussed. Furthermore, our results showed that La doping greatly enhanced the remnant polarizations.

1 Introduction

Multiferroic materials have recently attracted considerable attention due to their simultaneous effects of ferroelectricity, ferromagnetism, and ferroelasticity [1, 2]. Hence, they presents many opportunities for fundamental study and potential applications in information storage, spintronics, and sensors [3, 4]. As one of single-phase multiferroics, perovskite bismuth ferrite ($BiFeO_3$, BFO) has been extensively studied due to its two robust ferroic phase transitions well above room temperature (i.e., 370 °C for the Neel temperature and 830 °C for the Curie temperature) [5, 6]. However, the high leakage current density is one of the most important obstacles for BFO practical applications in devices because the BFO material is fabricated usually accompanying the production of the impurities such as $Bi_2Fe_4O_9$, $Bi_{25}FeO_{40}$, $Bi_{36}Fe_2O_{57}$ etc. [7]. Moreover, the antiferromagnetic BFO has a spiral modulated spin structure in the period of 62 nm, which greatly lowers macroscopic magnetization and also inhibits the observation of linear magnetoelectric effect in bulk BFO [8]. Many attempts have been done recently to overcome these shortcomings. For example, nitric acid leaching method was used to eliminate impurity phases in the solid-state route [9]. But, unfortunately, this method would result in coarser crystallites and had poor reproducibility. Several alternative chemical synthesis routes, such as ferrioxalate precursor method [10], co-precipitation method [11], the soft chemical route [12], solvothermal process [13], sol–gel process [14], polymeric precursor method [15] and so on, have been proposed to synthesize single phase $BiFeO_3$ or BLFO. However, these chemical methods still need an additional calcined process at >400 °C, and also results in irregular morphology and broad distribution of particle sizes. Moreover, rare-earth or transition metal ions, such as Cr^{3+}, Ti^{4+}, Mn^{3+}, La^{3+} etc. for Bi^{3+} and Fe^{3+} ions have been utilized to increase phase stability and enhance electrical and magnetic properties of $BiFeO_3$ [16–19]. It was reported that using La^{3+} substitution, the spiral modulated spin structure in BFO could be partially destroyed, and the spatial homogenization of spin arrangement could

Z. Chen (✉) · Y. Li · Y. Wu
College of Materials Science and Engineering, South China University of Technology, Guangzhou 510640, People's Republic of China
e-mail: chenzw@scut.edu.cn

Z. Chen
State Key Laboratory of Advanced Technology for Materials Synthesis and Processing, Wuhan University of Technology, Wuhan 430070, People's Republic of China

J. Hu
College of Chemistry and Chemical Engineering, South China University of Technology, Guangzhou 510640, People's Republic of China

be realized causing the magnetic property of BFO to increase [10, 19].

As a method for synthesizing high quality crystallite, hydrothermal method has many advantages in comparison with other techniques, such as low processing temperature, high crystallinity degree, well-controlled morphology, high purity, and narrow size distribution [20].

In the present study, $Bi_{1-x}La_xFeO_3$ crystallites were prepared by hydrothermal method. The effect of the hydrothermal parameters including precursor composition, alkali concentration, and reaction temperature and time on the crystallinity and morphology of BLFO crystallites were investigated systematically. Furthermore, a fundamental understanding of the formation mechanism is crucial for the rational design and controlled synthesis of these materials. So, the growth mechanism of the BLFO crystallites was also discussed.

2 Experimental procedure

In a typical procedure for the preparation of La-doped bismuth ferrite ($Bi_{1-x}La_xFeO_3$, x = 0, 0.15, 0.3, and 0.4) crystallites, bismuth nitrate ($Bi(NO_3)_3{\cdot}5H_2O$), lanthanum nitrate ($La(NO_3)_3{\cdot}6H_2O$), and iron nitrate ($Fe(NO_3)_3{\cdot}9H_2O$) were first dissolved in diluted nitric acid (HNO_3) to form aqueous solutions according to the stoichiometric proportion of $Bi_{1-x}La_xFeO_3$. Then, the 10 M potassium hydroxide (KOH) solution was slowly added into the above solution to induce a co-precipitation reaction, in which a brown precipitate was formed under stirring. The brown precipitate was filtered and washed with distilled water to remove NO_3^{-1} and K^+ ions. Then, the precipitate was mixed with 60 ml KOH solution under constant magnetic stirring for 10 min. KOH concentrations were varied from 4 to 12 M. Finally, the as-prepared suspension solution was sealed in a Teflonlined stainless steel autoclave with a filling capacity of 80% under different temperatures (from 100 to 200 °C) and time (form 1 to 24 h). After cooling, the products were filtered, washed with distilled water, and dried at room temperature.

Crystalline structures of the $Bi_{1-x}La_xFeO_3$ particles were examined using an X-ray diffractometer (XRD, D/Max-3C, Japan) with Cu Kα radiation. The morphologies of the synthesized $Bi_{1-x}La_xFeO_3$ particles were observed by a Scanning electron microscopy (SEM, LEO 1530 VP, Germany), and the composition of BLFO was roughly examined by using energy dispersive spectroscopy (EDS) attached with SEM. Infrared spectra were measured by using a Nicolet-Nexus 670 FTIR spectrometer from 400 to 4,000 cm^{-1}. Differential thermal analysis (DTA, STD Q600) of BLFO crystallites was carried out in nitrogen ambient at a scan rate of 10 °C min^{-1}. Polarization–electric field hysteresis loops were measured using a ferroelectric test system (Radiant Precision Premier II, USA).

3 Results and discussion

Figure 1 shows XRD patterns of $Bi_{1-x}La_xFeO_3$ crystallites (x = 0, 0.15, 0.3, 0.4) synthesized using 12 M KOH at 180 °C for 20 h. It could be seen from Fig. 1 that when x was equal to 0, 0.15, and 0.3, all diffraction peaks could be indexed as a pure BFO phase with a rhombohedrally distorted perovskite structure (JCPDS: 86-1518, R3c space group). No other phases could be discerned in Fig. 1 indicating that La^{3+} ions had doped into the perovskite lattice to form a solid solution. It is especially important to note that well-crystallized pure BLFO crystallites could be obtained when x was less than 0.3. Further increasing the quantity of La doping (x = 0.4), a small amount of impurity-phases $Bi_2Fe_4O_9$ was easily discerned. In addition, the diffraction peaks of BLFO had a slight shift to small angle as compared with that of BFO, which may result from the difference of ionic radius of Bi^{3+} (r = 1.14 Å) and La^{3+} (r = 1.22 Å) ions.

To further analyze the structure, the FT-IR spectra of the $Bi_{0.7}La_{0.3}FeO_3$ crystallites was measured, as shown in Fig. 2. As we know, the bands between 700 and 400 cm^{-1} were mainly attributed to the formation of metal oxides, while the peaks at 560 and 440 cm^{-1} in the $Bi_{0.7}La_{0.3}FeO_3$ crystallites assigned to the mode of stretching vibrations along the Fe–O axis and the mode of the Fe–O bending vibration, being characteristics of the octahedral FeO_6 groups in the perovskite compounds [10]. The formation of perovskite structure can be confirmed by the presence of metal–oxygen band [21]. The broad band between 3,600 and 3,000 cm^{-1} was attributed to the antisymmetric and

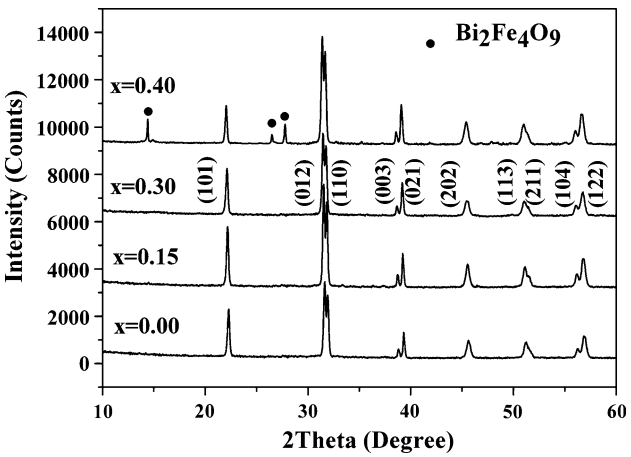

Fig. 1 XRD patterns of $Bi_{1-x}La_xFeO_3$ crystallites (wherein, x = 0, 0.15, 0.3, and 0.4) synthesized using 12 M KOH at 180 °C for 20 h

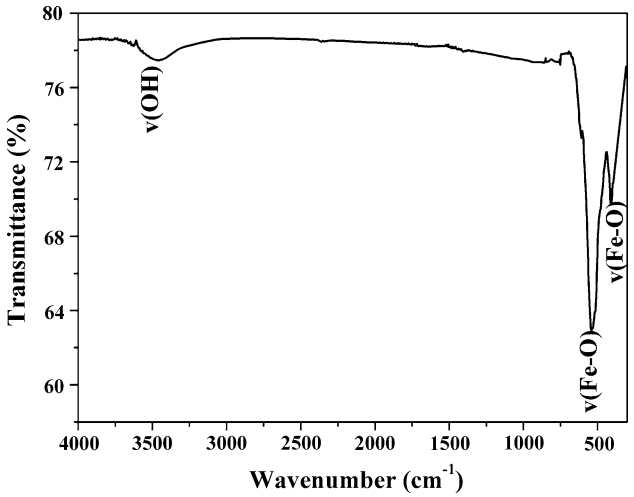

Fig. 2 FT-IR spectra of $Bi_{0.7}La_{0.3}FeO_3$ crystallites prepared using 12 M KOH at 180 °C for 20 h

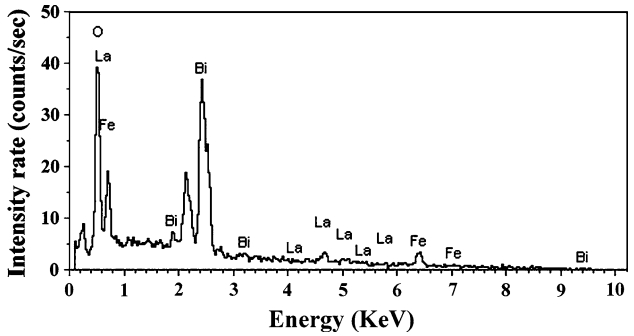

Fig. 3 EDS spectrum of $Bi_{0.7}La_{0.3}FeO_3$ crystallite prepared using 12 M KOH at 180 °C for 20 h

symmetric stretching of bond H_2O and OH^{-1} groups [22], which may be due to the absorption of water molecules from the air. In order to confirm La doping in BLFO crystallites, EDS analysis was performed. Fig. 3 shows EDS spectrum of $Bi_{0.7}La_{0.3}FeO_3$ crystallite. The appearance of La element and the atom ratio (2.5) of Bi to La revealed that the La^{3+} ions had successfully been doped into BFO. Moreover, it has been known that La-doped impurity phase could not be detected from the XRD patterns (Fig. 1), disclosing that the La^{3+} ions had occupied the lattice position in BLFO crystallites.

Figure 4 shows SEM images of $Bi_{1-x}La_xFeO_3$ ($0 \leq x \leq 0.4$) particles synthesized using 12 M KOH at 180 °C for 20 h. It could be clearly seen from Fig. 4 that the morphologies of the BLFO associated with the quantity of lanthanum doping. The $BiFeO_3$ particles were mainly spherical shape with the average diameter of 30 μm. In addition, the surfaces of the particles were rough, as shown in Fig. 3a. When La^{3+} ions were doped, the particles still retained the sphere-like shape at $x = 0.15$ Fig. 3b, but the average diameters of particles decreased to 20 μm and the smoother surface was obtained in comparison with the BFO. When 0.3 La^{3+} was doped, the particle morphology was octahedral shape and the average particle size was around 15 μm, as shown in Fig. 3c. Figure 3d shows SEM image of the BLFO sample ($x = 0.4$), in which the BLFO crystallite had irregular shape and easily gathered into large particles. To sum up, La^{3+} doping played a critical role in the morphologies and dimensions of the BLFO.

Figure 5 shows XRD patterns of $Bi_{0.7}La_{0.3}FeO_3$ crystallites synthesized at 180 °C for 20 h using different KOH concentrations from 1 to 14 M. It was clear that the $Bi_{0.7}La_{0.3}FeO_3$ phase with a perovskite structure was synthesized when the KOH concentrations were 1 and 2 M, but a small amount of impurity-phase $Bi_2Fe_4O_9$ was also detected. With increasing KOH concentration up to the range of 4–12 M, the diffraction peaks of the impurity phases disappeared completely. However, further increasing KOH concentration up to 14 M, the diffraction peaks of BLFO became weaker, and the (202), (113), and (211) peaks disappeared, which implied that high alkali concentration would lower the crystallinity of BLFO crystallites. It should be related to the reaction decay resulting from the rapid consumption of hydroxides in the supersaturated fluids at high alkali concentration. Above XRD results indicated that pure $Bi_{0.7}La_{0.3}FeO_3$ crystallite could be synthesized when the KOH concentration was in the range of 4–12 M.

To study the influence of reaction temperature on the sizes and morphologies of $Bi_{0.7}La_{0.3}FeO_3$ crystallites, different reaction temperatures (120, 140, 160, 180, and 200 °C) were used. Their XRD patterns are shown in Fig. 6. It can be seen that pure phase BLFO crystallites were obtained at the temperature range of 160–200 °C. While 100 and 120 °C were employed, the $Bi_{36}Fe_2O_{57}$ phases (JCPDS No. 42-181) with cubic structure were obtained, indicating that lower temperature would be apt to the formation of $Bi_{36}Fe_2O_{57}$ impurity phases whereas high temperature was necessary to form pure BFO perovskite phase. Compared with previous methods [14], the hydrothermal method successfully lowered the synthesis temperature from 600 to 160 °C, which may be because that the hydrothermal environment remarkably accelerated the reaction kinetics. In addition, we also studied the influences of reaction time on the synthesis of BLFO. Figure 7 shows XRD patterns of $Bi_{0.7}La_{0.3}FeO_3$ particles synthesized at 180 °C using different reaction time. Our results indicated that there existed a small amount of amorphous and partially crystalline structure in BLFO powders synthesized using 1 or 4 h, and full crystalline was obtained after 8 h. With increasing reaction time, the diffraction peaks of $Bi_{0.7}La_{0.3}FeO_3$ particles become sharper and stronger, revealing that well-crystallized $Bi_{0.7}La_{0.3}FeO_3$ particles could be synthesized in the range of 8 and 20 h. However,

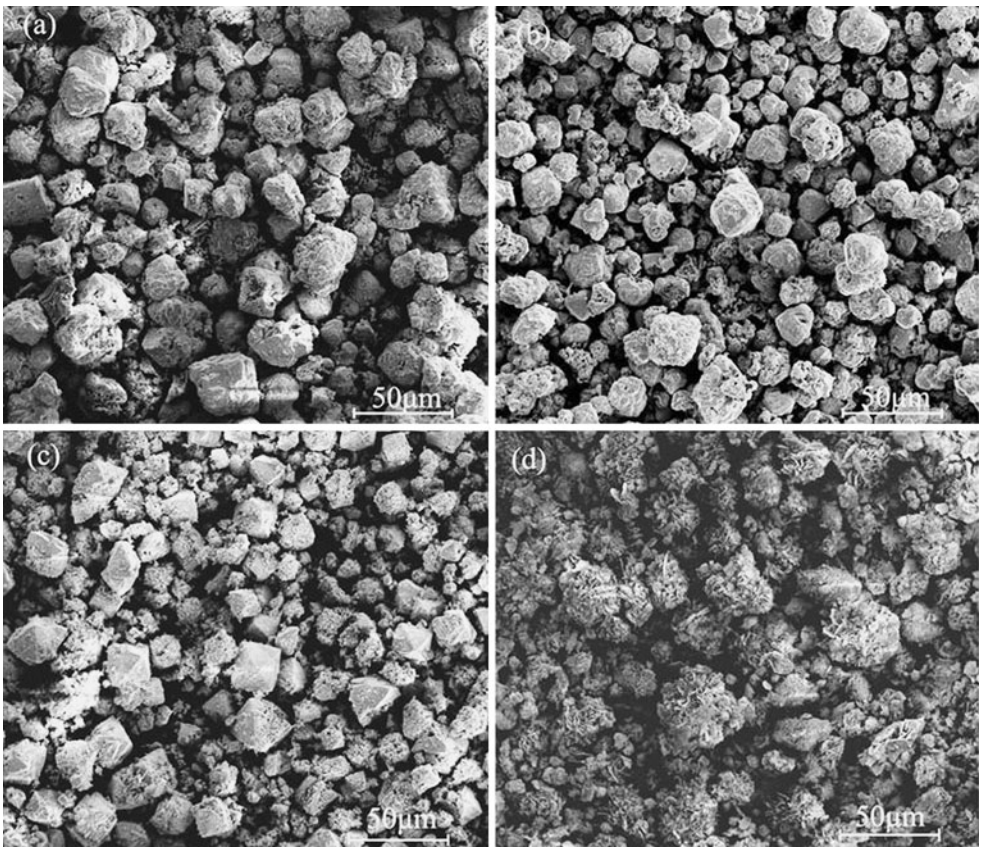

Fig. 4 SEM images of $Bi_{1-x}La_xFeO_3$ crystallites in which x is **a** 0, **b** 0.15, **c** 0.3, and **d** 0.4, respectively

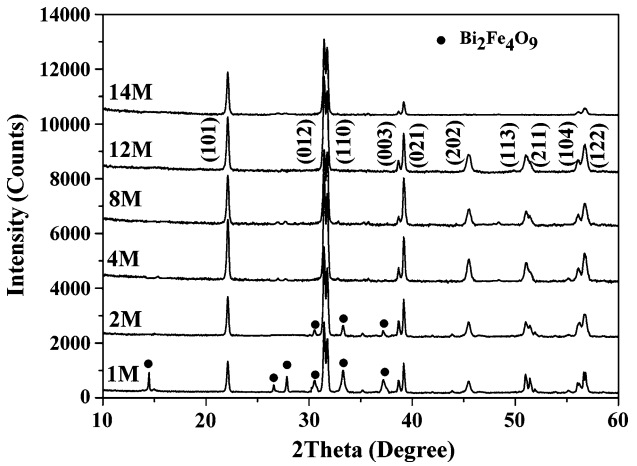

Fig. 5 XRD patterns of $Bi_{0.7}La_{0.3}FeO_3$ crystallites synthesized at 180 °C for 20 h using different KOH concentrations of 1, 2, 4, 8, 12 and 14 M, respectively

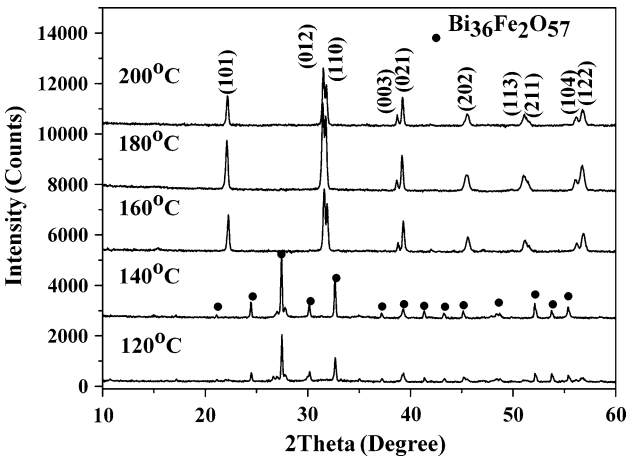

Fig. 6 XRD patterns of $Bi_{0.7}La_{0.3}FeO_3$ crystallites synthesized using 12 M KOH for 20 h at 120, 140, 160, 180, and 200 °C, respectively

the peak intensity decreased when the hydrothermal time is more than 20 h, which is related to the reaction decay resulting from the rapid consumption of hydroxides in the supersaturated fluids at high temperature.

Our results suggested that the $Bi_{1-x}La_xFeO_3$ formation possibly involved two stages: (1) the nitrates transformed into hydroxide precipitations after adding KOH; (2) $Bi(OH)_3$, $La(OH)_3$, and $Fe(OH)_3$ reacted with each other to form BLFO under hydrothermal environment. However, at this stage, besides BLFO, the impurity $Bi_2Fe_4O_9$ and $Bi_{36}Fe_2O_{57}$ crystallites perhaps formed under the appropriate hydrothermal conditions. The formation process could be possible expressed as following formula:

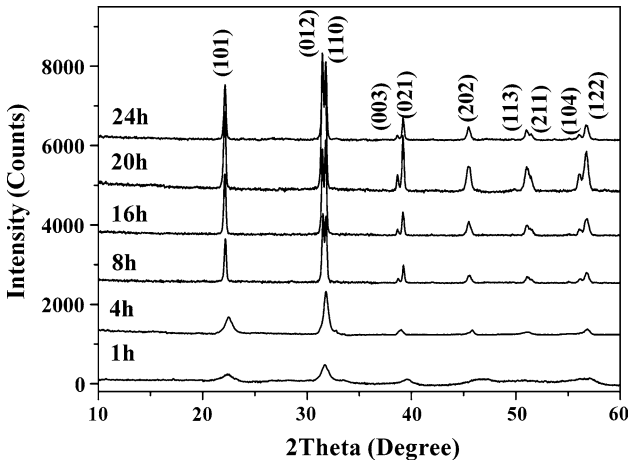

Fig. 7 XRD patterns of $Bi_{0.7}La_{0.3}FeO_3$ crystallites synthesized using 1, 4, 8, 16, 20, and 24 h, respectively

$$Bi(NO_3)_3+La(NO_3)_3+Fe(NO_3)_3+9KOH \rightarrow Bi(OH)_3+Fe(OH)_3+La(OH)_3+9KNO_3 \quad (1)$$

$$(1-x)Bi(OH)_3+xLa(OH)_3+Fe(OH)_3 \rightarrow Bi_{1-x}La_xFeO_3+3H_2O \quad (2)$$

$$2Bi(OH)_3+4Fe(OH)_3 \rightarrow Bi_2Fe_4O_9+9H_2O \quad (3)$$

$$36Bi(OH)_3+2Fe(OH)_3 \rightarrow Bi_{36}Fe_2O_{57}+57H_2O \quad (4)$$

"Dissolution–crystallization" has been considered to be a basic mechanism to describe the hydrothermal process [23, 24], in which the dissolution of the reactants is strongly dependent on a mineralizer and crystallization only occurring in the supersaturated fluid. Dissolution takes place when the reactants are loaded and heated in a hydrothermal system; then, more stable phases precipitate once the supersaturation for the phases is achieved. In our hydrothermal system, when KOH was used as a mineralizer, the hydroxide precipitations, such as $Bi(OH)_3$, $Fe(OH)_3$, and $La(OH)_3$ as shown in Eq. 1 were dissolved in an alkali solution under high temperature and pressure. Under the suitable hydrothermal atmosphere, $Bi(OH)_3$, $La(OH)_3$ would react with $Fe(OH)_3$, as shown in Eq. 2. Supersaturation of BLFO was achieved when a sufficient amount of BLFO nuclei was dissolved in the whole bulk solution. As we all know, crystal growth only occurred in the region of supersaturated fluid. So, the crystalline BLFO particles were formed by nucleation, precipitation, dehydration and growth, as soon as supersaturation was achieved. It is well-known that the size and morphology of the product depend strongly on both crystal nucleation and crystal growth. At the beginning of the crystal growth process, very small particles (~a few nanometers) were formed, which were usually spherical shape [25]. At $x = 0$ and 0.15, these spherical nanoparticles further grew into spherical microstructure (Fig. 4a, b). If the La doping increased up to $x = 0.3$, the spherical nanoparticles further grew into octahedral-shape particles (Fig. 4c), which might be because La doping offered additional energy for a certain crystal plane to grow fast.

As we mentioned above, the hydroxide precipitations were dissolved in aqueous solution to form BLFO nuclei during hydrothermal process. Supersaturation was achieved when a sufficient amount of BLFO ions was dissolved in the whole bulk solution, which was of importance because both requirements of supersaturation and stoichiometry for the ions to form BLFO crystallites must be satisfied. If the conditions were carefully adjusted during the hydrothermal process, a second phase would not form. Therefore, the dissolution and crystallization process continued in supersaturated fluid in such a way that the system was self-stabilizing. As for specimens synthesized with the KOH concentrations of 4, 8, and 12 M, the amount of KOH was appropriate and beneficial for the formation of pure BLFO. While, when the KOH concentrations were 1 and 2 M, the balance of dissolution and crystallization process for pure BLFO were destroyed because the pH value was changed. At this time, as shown in Eq. 3, a sufficient amount of component (containing $Bi_2Fe_4O_9$) ions were dissolved in the whole bulk solution, therefore, the supersaturation of $Bi_2Fe_4O_9$ was achieved. Similarly, when crystallite samples synthesized at 100 and 120 °C, the formation of $Bi_{36}Fe_2O_{57}$ impurity phases was favored at the two lower treatment temperatures. So, as shown in Eq. 4, the supersaturation of $Bi_{36}Fe_2O_{57}$ was achieved. Thus, the impurity phases, such as $Bi_2Fe_4O_9$ or $Bi_{36}Fe_2O_{57}$ crystallites were formed and detected in XRD patterns, as shown in Figs. 5 and 6.

The DTA curves shown in Fig. 8 revealed the endothermic peaks at around 830 °C for BLFO crystallites synthesized using different La doping, which arise from the ferroelectric to paraelectric phase transformation, indicating one of evidences of the ferroelectricity of BLFO crystallites. This value is match well with the 836 °C of $BiFeO_3$ crystallites reported by Kim et al. [14]. It could be seen that the ferroelectric transition temperature of BLFO decreased from 834.2 to 828.7 °C with increasing La doping. It was reported that perovskite materials have high T_c values when the tolerance factor, t, was small [26]. The substitution of larger La^{3+} for Bi^{3+} ions in BFO lattice would increase t, which was a possible explanation of the lower T_c value for the lanthanum-doped BFO compounds [26]. In order to detect the ferroelectric properties, the as-prepared BLFO crystallite was hot-pressed (with a pressure of 15 MPa) into pellets using polyvinyl alcohol (PVA, at a concentration of 6%) as binding agent (the mass ratio of PVA was 3%) for ferroelectric measurement [27]. The ferroelectric hysteresis loops of BLFO crystallites synthesized at 180 °C for 20 h are shown in Fig. 9. It was clear

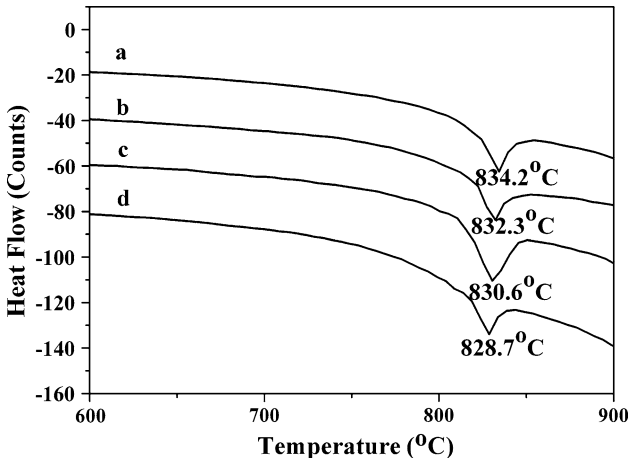

Fig. 8 DTA curves of $Bi_{1-x}La_xFeO_3$ crystallites in which x equals *a* 0, *b* 0.15, *c* 0.3, and *d* 0.4, respectively

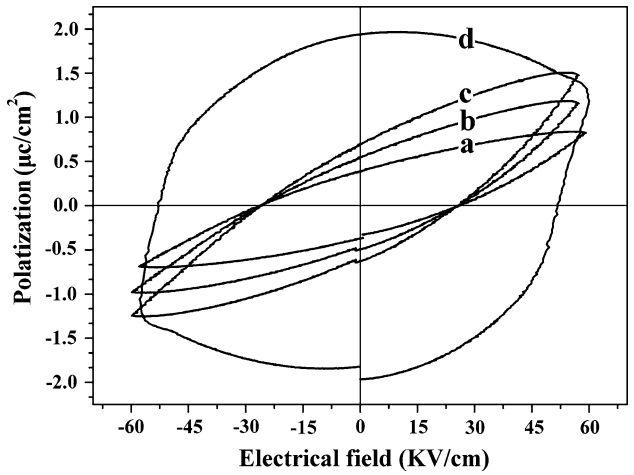

Fig. 9 *P–E* loop of the $Bi_{1-x}La_xFeO_3$ crystallites in which x equals *a* 0, *b* 0.15, *c* 0.3, and *d* 0.4, respectively

that when $x = 0.4$, the *P–E* loop of $Bi_{0.6}Fe_{0.4}O_3$ were measured as circles, which meant the sample had serious electrical leakage. While, typical *P–E* loops were displayed at room temperature under an applied field of ±60 kV cm^{-1} for $x = 0$, 0.15 and 0.3, which meant the electric leakage was greatly reduced. The typical *P-E* loops indicate ferroelectric behavior for the BLFO crystallites synthesized have been achieved (since PVA was nonferroelectric). It can be seen that the remnant polarization (P_r) increased along with the La doping. The substitution of larger La^{3+} for Bi^{3+} ions would lead to distortion in BFO lattice. The higher quantity of La^{3+} was doped, the larger degree of distortion would be generated. This distortion of the BFO lattice might lead to an increase in polarization ability in the form of remnant polarization. Since all La doped samples had higher distortion than the un-doped samples, the remnant polarizations were larger in the doped samples. Moreover, the sample with $x = 0.3$ had the greatest remnant polarization because of its largest distortion. In addition, it can be seen from Fig. 9 that the significant inhibition of electrical leakage has been presented in single phase BLFO. We propose that the formation of a second phase, such as $Bi_2Fe_4O_9$, resulted in charge unbalance in the $Bi_{0.6}Fe_{0.4}O_3$ specimen. As a result, a large amount of defects, such as oxygen vacancies and variant valence ions, would form and thus increased the conductivity of the samples.

4 Conclusions

In summary, we have successfully synthesized $Bi_{1-x}La_xFeO_3$ (BLFO, $x = 0$, 0.15, 0.3, 0.4) crystallites by hydrothermal method. It was found that pure BLFO crystallites could be obtained when x was less than 0.3. The morphologies of the obtained particles were sphere-like when $x \leq 0.15$ and changed into octahedral as $x = 0.3$. The XRD results demonstrated that the appropriate KOH concentration was beneficial for the formation of pure BLFO, and the reaction temperature and time played an important role on the formation of BLFO crystallites. A dissolution–crystallization process was also discussed to explain the formation of the BLFO crystallites. The ferroelectric measurement showed that La doping greatly enhanced the remnant polarizations.

Acknowledgments The project was supported by National Natural Science Foundation of China (No. 50702022), the Fundamental Research Funds for the Central Universities, SCUT (Nos. 2012ZZ0008; 2009ZM0015), State Key Laboratory of Pulp and Paper Engineering (South China University of Technology, Nos. 200901, 200904) and State Key Lab of Advanced Technology for Materials Synthesis and Processing (Wuhan University of Technology, No. 2010-KF-4).

References

1. M. Fiebig, J. Phys. D Appl. Phys. **38**, R123–152 (2005)
2. W. Eerenstein, N.D. Mathur, J.F. Scott, Nature **442**, 759–765 (2006)
3. N. Hur, S. Park, P.A. Sharma, J.S. Ahn, S. Guha, S.W. Cheong, Nature **429**, 392–395 (2004)
4. N.A. Spaldin, M. Fiebig, Science **309**, 391–392 (2005)
5. J. Wang, J.B. Neaton, H. Zheng, V. Nagarajan, S.B. Ogale, B. Liu et al., Science **299**, 1719–1722 (2003)
6. S.M. Selbach, T. Tybell, Adv. Mater. **20**, 3692–3696 (2008)
7. T.T. Carvalho, P.B. Tavares, Mater. Lett. **62**, 3984–3986 (2008)
8. I. Sosnowska, T. Peterlin-Neumaier, J. Phys. C Solid State Phys. **15**, 4835–4846 (1982)
9. M.M. Kumar, V.R. Palkar, K. Srinivas, S.V. Suryanarayana, Appl. Phys. Lett. **76**, 2764–2766 (2000)
10. S. Kazhugasalamoorthy, P. Jegatheesan, R. Mohandoss, N.V. Giridharan, B. Karthikeyan, R.J. Joseyphus et al., J. Alloy Compd. **493**, 569–572 (2010)

11. S. Shetty, V.R. Palkar, R. Pinto, Pramana, J. Phys. **58**, 1027–1030 (2002)
12. S. Ghosh, S. Dasgupta, A. Sen, H.S. Maiti, J. Am. Ceram. Soc. **88**, 1349–1352 (2005)
13. A. chaudhuri, S. Mitra, M. Mandal, K. Mandal, J. Alloy. Compd. **491**, 703–706 (2010)
14. J.K. Kim, S.S. Kim, W.J. Kim, Mater. Lett. **59**, 4006–4009 (2005)
15. A.Z. Simões, F.G. Garcia, C.D. Riccardi, Mater. Chem. Phys. **116**, 305–309 (2009)
16. H. Naganuma, J. Miura, S. Okamura, Appl. Phys. Lett. **93**, 052901 (2008)
17. Y. Wang, C.W. Nan, Appl. Phys. Lett. **86**, 052903 (2006)
18. V.R. Palkar, D.C. Kundaliya, S.K. Malik, J. Appl. Phys. **93**, 4337–4339 (2003)
19. Y.H. Lin, Q.H. Jiang, Y. Wang, C.W. Nan, Appl. Phys. Lett. **90**, 172507 (2007)
20. Q.B. Yang, Y.X. Li, Q.R. Yin, P.L. Wang, Y.B. Cheng, J. Eur. Ceram. Soc. **23**, 161–166 (2003)
21. O. Yamaguchi, A. Narai, T. Komatsu, K. Shimizu, J. Am. Ceram. Soc. **69**, 256–257 (1986)
22. A.C. Tas, P.J. Majewski, F. Aldinger, J. Am. Ceram. Soc. **83**, 2954–2960 (2000)
23. Z.W. Chen, G.H. Zhan, X.H. He, H. Yang, H. Wu, Cryst. Res. Technol. **46**, 309–314 (2011)
24. C.R. Peterson, E.B. Slamovich, J. Am. Chem. Soc. **82**, 1702–1710 (1999)
25. J.T. Han, Y.H. Huang, X.J. Wu, C.L. Wu, W. Wei, B. Peng et al., Adv. Mater. **18**, 2145–2148 (2006)
26. J.R. Cheng, R. Eitel, L.E. Cross, J. Am. Ceram. Soc. **86**, 2111–2115 (2003)
27. J.T. Wu, S.Y. Mao, Z.G. Ye, Z.X. Xie, L.S. Zheng, J. Mater. Chem. **20**, 6512–6516 (2010)